Article

A Compact Native 24-Residue Supersecondary Structure Derived from the Villin Headpiece Subdomain

Henry G. Hocking, ^{1,2} Florian Häse, ³ Tobias Madl, ^{1,2,4} Martin Zacharias, ³ Matthias Rief, ^{5,6} and Gabriel Žoldák^{5,*}

¹Center for Integrated Protein Science Munich, Department Chemie, Technische Universität München, Garching, Germany; ²Institute of Structural Biology, Helmholtz Zentrum München, Neuherberg, Germany; ³Physik-Department T38, Technische Universität München, Garching, Germany; ⁴Institute of Molecular Biology & Biochemistry, Center of Molecular Medicine, Medical University of Graz, Graz, Austria; ⁵Physik Department E22 and ⁶Center for Integrated Protein Science Munich, Physikdepartment, Technische Universität München, Garching, Germany

ABSTRACT Many small proteins fold highly cooperatively in an all-or-none fashion and thus their native states are well protected from thermal fluctuations by an extensive network of interactions across the folded structure. Because protein structures are stabilized by local and nonlocal interactions among distal residues, dissecting individual substructures from the context of folded proteins results in large destabilization and loss of unique three-dimensional structure. Thus, mini-protein substructures can only rarely be derived from natural templates. Here, we describe a compact native 24-residues-long supersecondary structure derived from the hyperstable villin headpiece subdomain consisting of helices 2 and 3 (HP24). Using a combination of experimental techniques, including NMR and small-angle x-ray scattering, as well as all-atom replica exchange molecular-dynamics simulations, we show that a variant with stabilizing substitutions (HP24stab) forms a densely packed and compact conformation. In HP24stab, interactions between helices 2 and 3 are similar to those observed in native folded HP35, and the two helices cooperatively stabilize each other by completing the hydrophobic core lining the central part of HP35. Interestingly, even though the HP24wt fragment shows a more expanded and less structured conformation, NMR and simulations demonstrate a preference for a native-like topology. Thus, the two stabilizing residues in HP24stab shift the energy balance toward the native state, leading to a minimal folding motif.

INTRODUCTION

Over the past two decades, the study of small proteins has provided us with important insights into the protein folding mechanism (1-7) supplemented by theoretical concepts of this mechanism based on the principle of minimal frustration and the funneled energy landscape (8–10). Examples include the speed limit of protein folding, the role of folding cooperativity, and residual structures in the unfolded state. Many small proteins fold via a cooperative two-state process and thus their native states are well protected from thermal fluctuations by a large kinetic barrier forged by an extensive network of interactions across the folded structure (11–13). The surprising observation that a relatively simple two-state model describes the folding mechanism of many small proteins (<100 aa) indicates that high cooperativity could be a vital attribute of proteins that evolved under natural selection and might be beneficial for their biological function (14–16). In turn, because cooperativity increases with size, short peptides may not be able to fold properly. Those arguments are supported by experimental findings that after individual peptides (<25 aa) are removed from folded protein domains (e.g., by protein dissection (17)), they usually cannot retain their native compact, well-packed confor-

Submitted July 25, 2014, and accepted for publication November 20, 2014. *Correspondence: gabriel.zoldak@tum.de

Editor: Ashok Deniz.

© 2015 by the Biophysical Society 0006-3495/15/02/0678/9 \$2.00

mation (18). However, rare exceptions with significant secondary structures are known (19,20). Moreover, the unstructured conformation of the peptide fragments is due to large unfavorable entropic penalties for folding (21), and hence only very few peptides can overcome such a burden. This means that as the repertoire of sequences increases, the protein will need a global stabilizing network of local and nonlocal interactions. Hence, high folding cooperativity is a logical consequence of the primary importance of sequence diversity for protein function. Thus, stable, uniquely folded mini-proteins can only rarely be derived from natural templates. In addition, the absence of sensitive experimental techniques makes the search for small, native-like folded peptide fragments challenging.

One of the best investigated small model proteins is the 35-residues-long villin headpiece subdomain (Fig. 1 A), which is part of the cytoskeletal multidomain protein villin (22). Its headpiece domain (HP67) is an actin-binding domain located at the C-terminus (23). McKnight et al. (24) found that when the last 35 residues are cleaved off, they retain their native structure, making this peptide a foldable helical subdomain without the need for any cofactor or disulfide bridges. By designing the villin headpiece subdomain HP35, Bi et al. (25) found that two amino acid substitutions in helix 3 result in a dramatic stabilization of the whole protein, producing a hyperstable protein

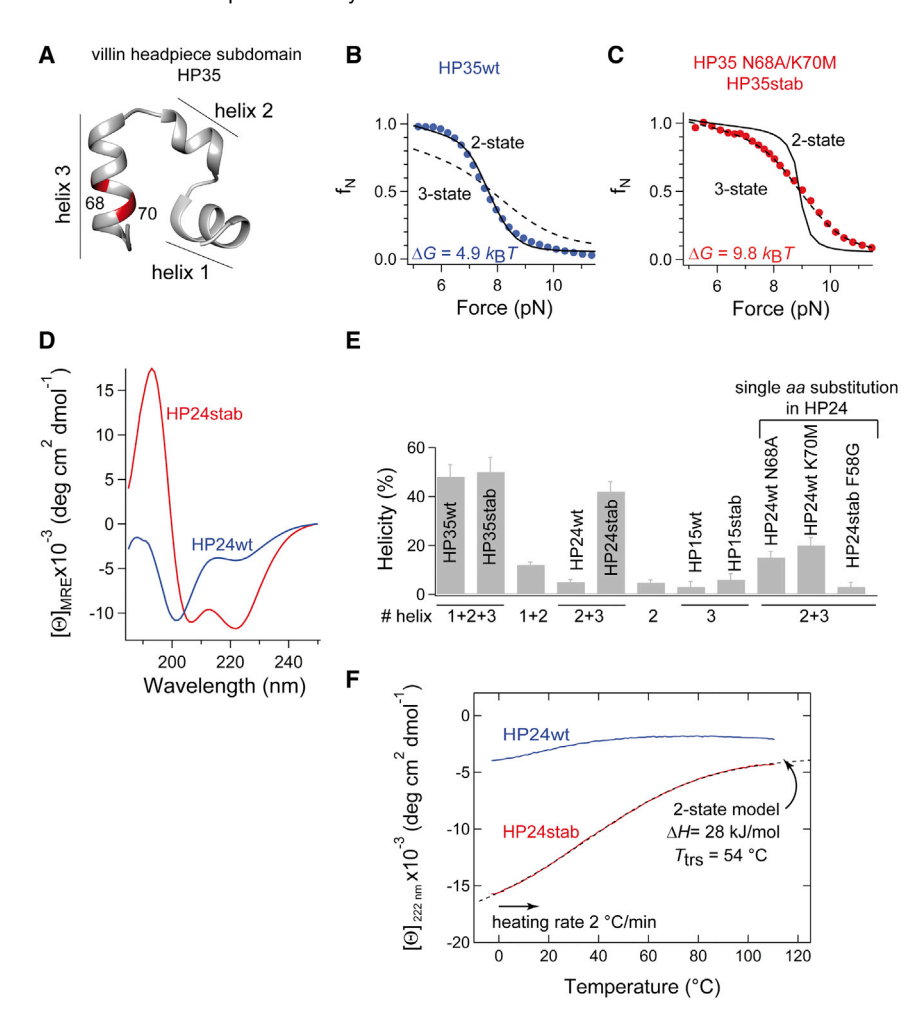


FIGURE 1 (A) Three-dimensional structure of the villin headpiece subdomain N68H HP36 (PDB 1YRF (51)). The positions of the residues N68 and K70 are shown in red. (B and C) Fraction of the native state calculated from single-molecule force experiments. The black lines are simulations of a two-state model (solid line) and three-state model (broken line) based on the parameters obtained from independent experiments. The data were taken from Žoldák et al. (26). (D) CD spectra in the far-UV region. The peptides were dialyzed in 5 mM sodium phosphate buffer (pH 7.0) at 25°C. For details, see Materials and Methods. (E) Helical content of HP35 and various truncated variants based on secondary structure analysis of their CD spectra performed by DICHROWEB (46,47). (F) Thermal denaturation of HP24stab (red) and HP24wt (blue) as measured at 222 nm at a scanning rate of $2^{\circ}\text{C} \times \text{min}^{-1}$ in 10 mM phosphate buffer, 2.7 mM potassium chloride, and 137 mM sodium chloride (pH 7.4). The protein concentration was 50 µM. The two-state analysis (black dashed line) results in $T_{trs} = 54.1 \pm 0.1$ °C and $\Delta H_{vH} = 28 \pm 1 \text{ kJ mol}^{-1}$. Because of the strong cooperativity between helix 2 and helix 3, as demonstrated by the nonadditivity of their helical contents, an analysis of the thermal denaturation of HP24stab by a one-dimensional helix-coil model would have been less appropriate. To see this figure in color, go online.

(~9 k_BT vs. ~4 k_BT for HP35wt from bulk denaturation experiments). This N68A/K70M HP35 construct, named HP35stab (numbered according to the headpiece domain), showed higher stability against chemical denaturation as well as mechanical loads in single-molecule force experiments using optical tweezers (26). These experiments revealed a difference in folding cooperativity between HP35wt and HP35stab. Whereas HP35wt is well described by a highly cooperative all-or-none transition, the folding transition of HP35 is much broader, indicating the presence of an equilibrium folding intermediate (Fig. 1, B and C). Our starting hypothesis was that the folding intermediate seen in the force experiments with HP35stab (26) should display sufficiently high stability to be observed upon isolation. The calculated contour length increase of 6.5 nm indicates that the intermediate consists of ~17-18 amino acid residues. Because the stabilizing mutations are located in helix 3, we designed several truncation variants of HP35 containing helix 3 as a scaffold and investigated them using circular dichroism (CD), NMR spectroscopy, small-angle x-ray scattering (SAXS), and theoretical all-atom molecular dynamics (MD) simulations. Our results show that the stabilizing residues in HP35stab shift the energetic balance such that a substructure containing the two C-terminal helices can fold independently, thus defining a minimal villin subdomain HP24stab. The broad spectrum of methods we used here provide unique structural insight into the mutual cooperativity of helices in HP24stab at atomic resolution.

MATERIALS AND METHODS

Materials

Tris, KCl, and EDTA were obtained from AppliChem (Germany), and other reagents were purchased from Merck (Germany) or Sigma-Aldrich. The peptides (95% purity) were synthesized by GenScript or Biomatik. The protein sequences of the peptides were as follows:

 $\label{eq:helix123wt} \mbox{ (HP35wt): LSDEDFKAVFGMTRSAFANLPLWKQQNLK KEKGLF}$

 $\label{eq:helix123stab} \mbox{ (HP35stab): LSDEDFKAVFGMTRSAFANLPLWKQQAL MKEKGLF}$

helix12: LSDEDFKAVFGMTRSAFANLPLWKQQ

helix23wt (HP24wt): MTRSAFANLPLWKQQNLKKEKGLF

helix23 (HP24stab): MTRSAFANLPLWKQQALMKEKGLF

helix3 (HP15wt): PLWKQQNLKKEKGLF

helix 3stab (HP15stab): PLWKQQALMKEKGLF

helix 2: MTRSAFANLP

The peptides were acetylated at the N-terminus and amidated at the C-terminus. Before use, they were dialyzed at 4°C against 2×1 liter of buffer

containing 20 mM sodium phosphate, 50 mM sodium chloride (pH 7.5) using Float-A-Lyzer G2 with a 100–500 Da cutoff (Spectra/Por).

CD experiments

CD experiments were conducted on a Jasco J-815 spectropolarimeter at 20°C using the following parameters: 1 nm bandwidth, scanning speed of 20 nm/min, 1 nm step resolution, 1 s response time, 0.1 cm path cuvette, and 25 accumulations. The peptides were dissolved in 0.1 M sodium phosphate (pH 7.0) and dialyzed overnight in 1 liter of 2 mM sodium phosphate (pH 7.5). The final concentration was determined by the absorbance at 280 nm (5500 M⁻¹cm⁻¹) for peptides containing a single tryptophan residue or at 230 nm for peptides with no tryptophan. Before analysis, the buffer baseline, measured under otherwise identical conditions, was subtracted. Heat-induced unfolding transitions were measured in a Jasco J-815 spectropolarimeter equipped with a PTC 348 WI peltier element at a peptide concentration of 50 μM in 10 mM phosphate buffer, 2.7 mM potassium chloride, and 137 mM sodium chloride (pH 7.4) at a heating rate of 2° C \times min⁻¹. The transitions were monitored by the increase of the CD signal at 222 nm with 2 nm bandwidth and 5 mm path length. The experimental data were analyzed on the basis of the two-state approximation (Eq. 3 in Mayr et al. (27)) and by assuming zero heat capacity change. Because of the strong cooperativity between helices 2 and 3, as demonstrated by the nonadditivity of their helical contents, an analysis of the thermal denaturation by a one-dimensional helix-coil model would have been less appropriate.

NMR spectroscopy

Samples of wild-type (wt) and the double mutant N16A/K18M of an N-terminal-truncated form of chicken villin headpiece (HP24wt; Protein Data Bank (PDB) 4CZ3) and HP24stab (PDB 4CZ4), respectively) were prepared for NMR in 20 mM sodium phosphate, 50 mM sodium chloride (pH 7.5). The peptide concentration was 3 mM and 10% $^{2}H_{2}O$ was used for the lock. Chemical shifts were referenced internally to the water frequency (28). Two-dimensional (2D) homonuclear total correlated spectroscopy (TOCSY) spectra with a spin-lock time of 100 ms and nuclear Overhauser effect spectroscopy (NOESY) spectra with mixing times of 100 and 250 ms were acquired at 298 K and 286 K on a Bruker AVANCE III 600 MHz spectrometer (Bruker Biospin) equipped with a 5 mm triple-resonance TXI z-gradient probe. Sequential spin systems were assigned based on H_{N} - $H_{N(i-1)}$ and H_{N} - $H_{\alpha(i-1)}$ NOE data. Standard natural abundance ¹H-¹³C heteronuclear single quantum coherence (HSQC), ¹H-¹⁵N HSQC, ¹⁵N-R₁ relaxation, and ¹⁵N-R₂ relaxation NMR spectra were acquired at 286 K on a Bruker AVANCE III 500 MHz spectrometer equipped with a 5 mm triple-resonance CPTCI z-gradient probe. ¹⁵N-R₂ relaxation data were recorded using a pulse sequence optimized for long T2 relaxation times (29). R1 data were recorded for both HP24wt and HP24stab using nine relaxation delay times (86.4, 162, 248.4, 345.6, 518.4, 669.6, 885.6, and 1144.8 ms). R₂ data were recorded for both HP24wt and HP24stab using seven relaxation delay times (76.7, 153.4, 230.1, 306.8, 383.6, 460.3, and 537 ms). Spectra were processed using TopSpin version 3.2 (Bruker Biospin) and analyzed using the Analysis software from the Collaborative Computing Project for the NMR community (30). Curve fitting of peak intensities to a function of the type A*exp(-Bx) was performed using the data analysis function in Ccpn Analysis. Fitting errors were estimated using the covariance error method. Peaks with substantial overlap were omitted from the analysis. We calculated the secondary chemical shift by using an in-house-written script and measuring the difference between the C_{α} chemical-shift deviation from random coil and the C_{β} chemical-shift deviation from random coil. To obtain temperature coefficients, we recorded a series of ¹H-¹³C HSQC and ¹H-¹⁵N HSQC spectra between 278 K and 343 K at 5 K increments.

Structure calculation

The structures of HP24wt and HP24stab were modeled and refined using CYANA 2.1 (31) from 100 initial randomized structures. Volumes of 1647 crosspeaks were determined from 2D NOESY spectra of HP24stab at 286 K and 298 K, resulting in a total of 558 upper-limit distance restraints. Volumes of 474 crosspeaks were determined from 2D NOESY spectra of HP24wt at 286 K and 298 K in 95% $\rm H_2O/5\%^{2}H_2O$, resulting in a total of 260 upper-limit distance restraints. For HP24stab, a total of 20 backbone dihedral angles and five χ_1 angle constraints were generated by TALOS-N (32) and added during the structure refinement. For HP24wt, a total of five backbone dihedral angles and seven χ_1 angle constraints were generated by TALOS-N and added during the structure refinement.

An ensemble of the 20 lowest-energy structures was then further refined in explicit water solvent using the RECOORD scripts for the software program CNS (33). The overall quality of the final structures was validated using the iCing webserver (34).

SAXS

All SAXS data were recorded on an in-house SAXS instrument (SAXSess mc2; Anton Paar, Graz, Austria) equipped with a Kratky camera, a sealed x-ray tube source, and a 2D Princeton Instruments PI•SCX:4300 CCD detector (Roper Scientific, Sarasota, FL). The scattering patterns were measured with a 180 min exposure time (1080 frames, each 10 s) for several solute concentrations in the range of 3–8 mg/ml. Radiation damage was excluded based on a comparison of individual frames of the 180 min exposures, where no changes were detected. A range of momentum transfers of $0.012 < s < 0.63 \text{ Å}^{-1}$ was covered ($s = 4\pi \sin(\theta)/\lambda$, where 2θ is the scattering angle and $\lambda = 1.5 \text{ Å}$ is the x-ray wavelength).

All SAXS data were analyzed with the package ATSAS (version 2.5). The data were processed with the SAXSQuant software (version 3.9) and desmeared using the programs GNOM (35) and GIFT (36). The forward scattering, I(0), radius of gyration, R_g , maximum dimension, D_{max} , and interatomic distance distribution functions, P(R), were computed with the programs GNOM and GIFT. The masses of the solutes were evaluated by comparison of the forward scattering intensity with that of a human serum albumin reference solution (molecular mass 69 kDa). The protein shapes were determined using the ab initio shape determination program DAMMIF (37). A total of 10 shapes were calculated and the averaged model was built using DAMAVER (38).

MD simulations

All simulations were performed with the GROMACS 4.5.3 software package (39). The force field AMBER99sb-ildn (40) was used for all peptide simulations. This force field is widely used in peptide and protein simulations, and long simulations on different types of proteins and peptides show good agreement with NMR-derived parameters for peptide conformation and dynamics (40). To generate the starting structures for HP24wt and HP24stab, a crystal structure of the entire villin headpiece (PDB code: 1YU5 (23)) was truncated to the residues M53–F76 (villin53–76, sequence: MTRSAFANLPLWKQQNLKKEKGLF). The mutations (Asn-68 to Ala-68, and Lys-70 to Met-70) were then introduced in silico by using the Mutagenesis Wizard of PyMol (41) and selecting the best-fitting rotamers. The systems were solvated in TIP3P water molecules (42) in a box with dimensions of (56 \times 56 \times 56) $\mathring{A}^3.$ Sodium and chloride ions were used to neutralize the system and to mimic experimental conditions. The total system size was 17,455 atoms and 17,464 atoms for HP24wt and HP24stab, respectively. Both setups were minimized for 50,000 steps. For temperature replica-exchange MD (T-REMD) simulations, we generated 21 replicas of the minimized structure and then equilibrated them in the isobaricisothermal ensemble for 150 ps at a constant pressure of 1 bar. We calculated the temperatures for each replica (listed in Table S2 in the Supporting Material) using a method proposed by Patriksson and van der Spoel (43). During the equilibration process, we restrained the peptides to the crystallographic structure by applying harmonic potentials with a force constant of 1000 kJ mol⁻¹ nm⁻². Unrestrained production runs were started for a total simulation time of 200 ns in each replica for both peptides. An exchange of replicas was attempted every 1 ps, which resulted in exchange acceptance rates of roughly 35% between neighboring replicas. We ensured convergence of the replica-exchange simulations by calculating the ratio of occupancy of each replica for all temperatures (Tables S3 and S4). Cluster analysis of the sampled conformations was performed based on the method of Daura et al. (44) as implemented in the GROMACS 4.5.3 software package. Clusters were defined by the number of neighbors within a root meansquare deviation (RMSD) cutoff of 0.2 nm, and the structure with the most neighbors was taken to represent the most frequently occurring cluster. All structures belonging to this cluster were then eliminated from the pool and the procedure was repeated for the next cluster (44).

Umbrella sampling (US) simulations were performed using the center-of-mass end-to-end distance between the first and last residues as the reaction coordinate. A harmonic distance-dependent penalty potential with a force constant of $240\,\mathrm{kJ}\,\mathrm{mol}^{-1}\,\mathrm{nm}^{-1}$ was used with a reference distance that varied between $1.2\,\mathrm{nm}$ and $2.7\,\mathrm{nm}$ in steps of $0.1\,\mathrm{nm}$. Distance distributions for each window were obtained from $40\,\mathrm{ns}$ simulations per window, resulting in a total simulation time of $640\,\mathrm{ns}$. The weighted histogram analysis method was used to calculate an associated potential of mean force (45).

RESULTS

Design and secondary structure content of the truncated HP35 variants

HP35 consists of three helices (helices 1–3; Fig. 1 A). In our first construct, we removed helix 1 from HP35wt and HP35stab, yielding HP24wt and HP24stab (Fig. 1 D) (26). We determined the helical content of the constructs from the analysis of far-UV CD spectra using DICHROWEB (Fig. 1 E) (46,47). For the wt background, deletion of residues corresponding to helix 1 in HP35 (residues 42–54; Fig. 1 A) resulted in a dramatic decrease of helicity, and the corresponding fragment, HP24wt, seemed to be largely in the unfolded conformation. In contrast, the HP24stab fragment, containing N68A/K70M residues, retained high helicity $(42\% \pm 4\%)$. Thus, the two residues in helix 3 stabilized this peptide fragment significantly, as we also confirmed by thermal denaturation experiments (Fig. 1 F). Thermal denaturation of HP24stab showed a very broad transition (red curve in Fig. 1 F) spanning 5–105°C. A two-state analysis of the thermal denaturation curve gave a melting temperature $T_{\rm trs}$ of ~54°C and a van't Hoff enthalpy of denaturation $\Delta H_D = 27 \text{ kJ mol}^{-1}$ at T_{trs} . Assuming a zero heat capacity change upon denaturation, the unfolding free energy at 20°C is ~2.9 kJ mol⁻¹. In contrast, the HP24wt variant showed no thermal transition (*blue curve* in Fig. 1 *F*).

To dissect the individual contributions of the N68A and K70M, we measured the helical content of HP24 N68A and HP24 K70M. Both residues showed a similar increase in helicity (~15% and 20% for HP24 N68A and HP24 K70M, respectively), which in combination yielded approximately the helical content of the double mutant HP24stab.

Hence, both stabilizing residues contributed roughly equally to the high helicity of the villin fragment. We also investigated the effect of helix 2 stability on the helicity of HP24stab (Fig. 1 *E*). When a flexible glycine residue was introduced, HP24stab destabilized dramatically and helical content decreased to 3%. The HP24stab F58G construct showed the typical spectrum of an unfolded peptide, which indicates that even though two stabilizing residues in helix 3 are present, destabilization of helix 2 results in a significant reduction of the helical structure.

Next, we removed residues corresponding to helix 2 in HP35 (residues 53–61; Fig. 1 A) from HP24, yielding the HP15wt and HP15stab constructs. A secondary structure analysis of these fragments (consisting essentially of the residues of helix 3) showed low helical content (6% and 3% for HP15wt and HP15stab, respectively). Intuitively, this result is expected for the wt background, but the low helicity of HP15stab is remarkable because the HP24stab fragment is highly helical and the two stabilizing residues are located within helix 3. Importantly, helix 2, which is the same in both backgrounds, shows a helicity of 4.7%. A plausible explanation is that in HP24stab, helix 3 interacts with helix 2 and thus both helices cooperate and stabilize each other, possibly in a similar way as in the native state. From the CD data, however, it is unclear whether these helices achieve a native-like fold or are engaged in a nonnative geometry with an eventually shifted pairing register. To address this issue, we undertook a detailed structural analysis using NMR spectroscopy and SAXS.

Conformational analysis of HP24 by NMR spectroscopy and SAXS

The natural-abundance ¹H-¹⁵N HSQC NMR spectra of HP24wt and HP24stab show good signal dispersion, as expected for folded proteins (Fig. 2 A). We observed large chemical-shift differences between HP24wt and HP24stab, indicating structural rearrangements. ¹H, ¹³C, and ¹⁵N chemical shifts of both forms were assigned using a combination of homonuclear (TOCSY and NOESY) and natural-abundance heteronuclear experiments (¹H-¹³C/¹⁵N HSQC) recorded at 286 K. Differences in secondary structure derived from ¹³C secondary chemical shifts are shown in Fig. 2 B. Overall, the secondary structure content is low in HP24wt, except for an α -helix between W64 and Q66. The N68A/K70M residues shift the ¹³C secondary chemical shifts toward more positive values and thus stabilize the α -helical conformation between residues L63 and K73 (Fig. 2 B). The stabilization of secondary structure can also be seen from the appearance of the NMR spectra and relaxation data (Supporting Material). The R_1 relaxation rates are of the same order for both forms, with somewhat higher values for HP24stab. Higher R2 relaxation rates extend farther toward the N-terminus in the double mutant form, indicating a more stable structure in this region compared with the wt.

682 Hocking et al.

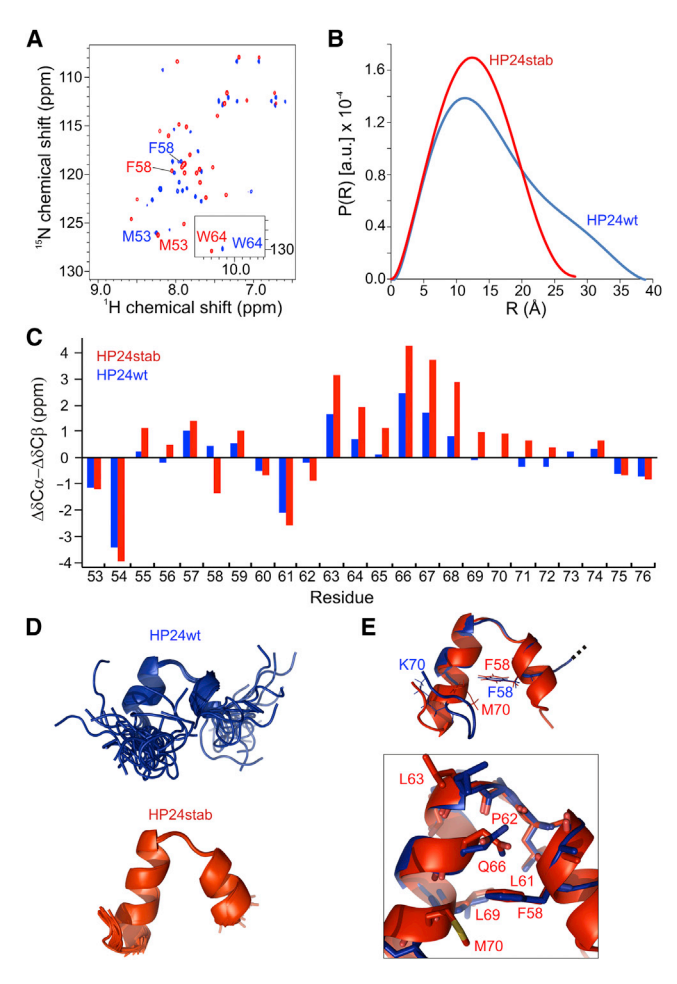


FIGURE 2 (A) ¹H-¹⁵N HSQC NMR spectra of HP24wt (*blue*) and HP24stab (*red*) of HP24 at 286 K. The tryptophan side-chain crosspeaks are shown as inlay and key residues are labeled. (B) SAXS data showing a comparison of the experimental radial density distributions of HP24wt and HP24stab. (C) Secondary chemical shifts for HP24wt (*blue*) and HP24stab (*red*). (D) Overlay of the lowest-energy NMR structures of HP24wt (*blue*) and HP24stab (*red*); core residues from both structures are highlighted in the right panel. (E) Upper panel: lowest-energy structures (cartoon) of HP24wt and HP24stab; F58 and M70/K70 are shown as sticks. Lower panel: overlay of the residues in the hydrophobic core of HP24wt and HP24stab. To see this figure in color, go online.

Rotational correlation times (τ_c) derived from the R_2/R_1 ratios show that HP24stab is less dynamic (higher τ_c) than HP24wt, as expected for a compact and tightly packed conformation. Temperature coefficients for amide protons and H α also support an extended and stable α -helix in HP24stab, with overall higher temperature coefficients and thus higher hydrogen-bond stability in this region compared with the wt (Fig. S4). This is in further agreement with the SAXS data. The radial density distributions show a clear difference between HP24wt and HP24stab. Whereas the wt protein shows an extended shape due to the higher degree of structural disorder ($D_{max} = 37 \ \text{Å}, R_g = 12 \ \text{Å}$), the mutant protein is more compact, showing a P(R) typical of a globular protein ($D_{max} = 28 \ \text{Å}, R_g = 10 \ \text{Å}$; Fig. 2 B). Based on

the NOE-based distance and angular restraints, we determined the structural ensembles of HP24stab and HP24wt with backbone RMSDs to the mean structure of 0.38 and 1.44 Å, respectively (for details and structural statistics, see Table S1 and Fig. S1). In contrast to HP24stab, the wt structural ensemble is less well defined at the N- and Ctermini, as reflected by the higher RMSD in these regions (see Fig. S1). This is due in large part to a paucity of NOE data for residues of the termini. In addition, no resonance assignments are available for S56 and K70. In this respect, it is likely that N- and C-termini form less stable structures in the wt than in the double mutant. However, the relaxation data (Figs. S2 and S3) do not seem to suggest that these regions are completely flexible, as might be inferred from the low convergence in the ensemble of structures. Given that these residues are extensively broadened, we conclude that they must undergo conformational exchange on the millisecond-microsecond timescale, which in turn would prohibit detection of NOEs.

In contrast to the double mutant, the first six and last five residues of HP24wt show poor structural convergence compared with the core region (residues 59–70). In this ensemble, a single, shorter α -helix appears between residues 64 and 69. Not only are there fewer restraints available for the wt, but they seem to be clustered in the core region of the peptide. F58, although well defined in the hydrophobic core of the peptide, does not appear to stabilize K70. Due to the lack of assignments for residue K70, no NOEs were found between these two residues (see Supporting Material). Two distinct α -helices (one between residues 56 and 61, and one between residues 64 and 74) are formed. The methyl group of M70, one of the mutations, is positioned in the hydrophobic core of the peptide and is potentially stabilized by the aromatic ring of F58 (Fig. 2 D).

The conformational analysis by NMR gave us a picture of a highly dynamic ensemble of interconverting structures in the case of HP24wt and a relatively stable, native-like conformation in the case of HP24stab. However, the origin of the higher thermodynamic stability of HP24stab remained unclear. Therefore, to study the structure-energetics-dynamics relationship at atomic resolution, we performed computational simulations.

T-REMD simulations of HP24wt and HP24stab

We employed MD simulations to study the dynamics and thermodynamics of HP24wt and HP24stab. To improve the sampling of possible conformational states, we conducted T-REMD in explicit solvent (Tables S2–S5). Simulations were started from the known experimental villin structure (PDB 1YU5) after truncation of the N-terminal residues and in silico generation of the N68A/K70M mutations. The T-REMD simulations were extended up to 200 ns in each of 20 replicas (temperature range 298–342 K), resulting in a total simulation time of 4 μ s. For both the

HP24stab and HP24wt fragments, a variety of conformations were sampled with an RMSD from the starting structure ranging from 0.2 (close to starting structure) to 0.8 nm (unfolded or partially folded conformations). The fraction of conformations close to the starting structure (within an RMSD of 0.2 nm) was significantly larger in the HP24stab variant than in the wt fragment (Fig. 3, A and B). The fluctuation and shift of residues along the protein chain was also larger for the HP24wt compared with the HP24stab variant in the T-REMD reference run (Fig. S6). If one considers conformations with RMSD < 0.3 nm as folded, one can estimate a difference of folding free energies for mutant versus wt of 4 kJ/mol based on the population along the RMSD coordinate. The NMR analysis of the wt and mutant fragments indicated a core part of the wt and mutant fragment with a defined structure (residues 53–71). The majority (90%) of sampled states during the simulations agreed with the NMR-derived structures, with an RMSD of ≤ 0.25 nm for residues 53-71 that were well defined in the NMR analysis (Supporting Material). Similar results were obtained using Hamiltonian REMD simulations (Supporting Material). Most of the conformational differences of the sampled states are due to the terminal segments that unfold partially or completely. A cluster analysis (see Materials and Methods) was used to identify frequently occurring conformations of both peptides throughout the trajectory.

Analysis of conformational clusters indicates that the most populated clusters still retain the overall folded backbone conformation of the central peptide segment (Fig. 3, C and D) (44). Notably, a contact between M70 and F58 is largely preserved in the most populated clusters of the mutant, forming part of a hydrophobic core region. In contrast, the corresponding K70 side chain in HP24wt is extruded from the core and is highly solvent exposed (Fig. 3 E). The contacts between M70 and F58 stabilize a hydrophobic core better than in the case of HP24wt.

To quantitatively estimate the free-energy difference between these two constructs, we performed US simulations to unfold the peptides along the end-to-end distance between the first and last residues (see Materials and Methods for details). Comparisons of the free-energy profiles indicate a larger free energy of unfolding of the mutant by 5 kJ mol⁻¹ compared with the wt, in accordance with the results from the T-REMD. For the mutant, we observed a metastable intermediate with ~18 kJ mol⁻¹ higher free energy than the folded form, showing a partially helical C-terminus, whereas we observed no intermediates for the wt along this unfolding path. However, presumably due to its higher energy (instability) and low barrier (~1 kJ mol⁻¹) along the reaction coordinate, such an intermediate was not observed in forced unfolding experiments. Hence, in accordance with the NMR analysis, US suggests a higher stability as well as a higher helicity for HP24stab.

DISCUSSION

A minimal headpiece subdomain, HP24stab

The discovery of the very stable and compact 35-residues-long villin headpiece subdomain has triggered intensive theoretical and experimental investigations (6,24–26,48–68). This subdomain has been used frequently as a test system for folding simulations in explicit solvent (3,48,57) and also for successful stable folding in an implicit solvent (69). The headpiece subdomain does not require additional metal ions or disulfide bridges to fold stably and exhibit a cooperative thermal unfolding transition. The small size of HP35 raised a fundamental question: how small can a stable structure be? Subsequently, a number of even shorter uniquely folded mini-proteins were found, as exemplified by Trpcage and Betanova, each consisting of only 20 aa residues (70,71). Interestingly, further attempts to prepare smaller

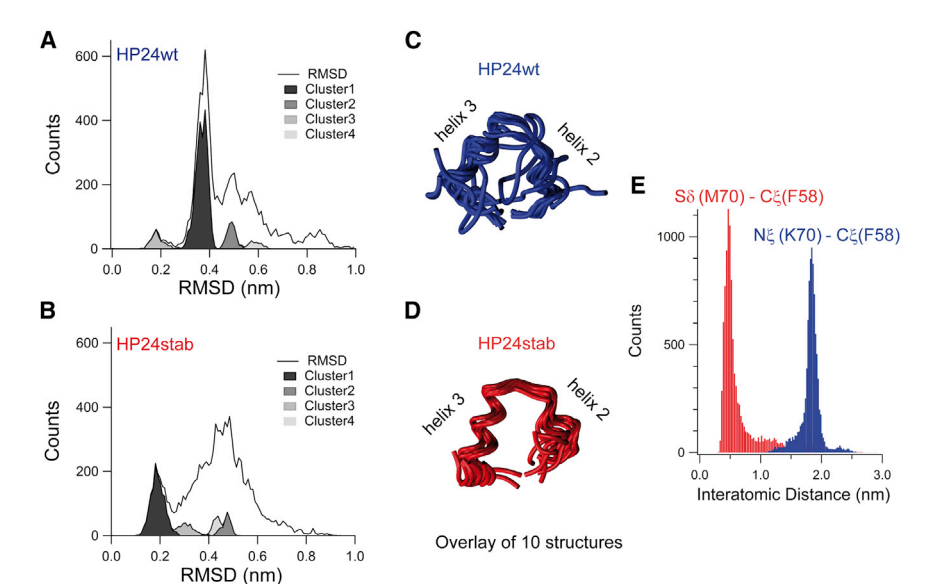


FIGURE 3 (A and B) RMSD distribution of reference replica at 298 K of the HP24wt (A) and HP24stab (B) with respect to the folded equilibrated structure. Smaller RMSD values correspond to conformations closer to the starting structure, and higher RMSD values indicate unfolded or partially unfolded conformations. Distribution regimes occupied by one particular cluster are colored in shades of gray according to their importance. Cluster analysis was performed according to the method of Daura et al. (44) using an RMSD cutoff between cluster centroids of 0.2 nm (see Materials and Methods). (C and D) Overlay of the representative structures of the 10 most populated clusters. (E) Distribution of the interatomic distances between individual atoms from the reference replica. To see this figure in color, go online.

684 Hocking et al.

thermodynamically stable folding units from HP35wt have failed. In isolation, the peptides corresponding to the residues of helices 1-3 of HP35wt are highly flexible and less structured, showing a transient residual structure with few native-like, long-ranged contacts (6,50,54,68). However, none of these peptide fragments show a compactly packed, unique core structure, and none resemble a well-folded protein. Here, we show that two stabilizing point mutations are sufficient to derive the shorter and well-packed, uniquely folded native-like motif, HP24stab. This 24-residues-long peptide displays the typical characteristics of folded proteins: it is very compact, is densely packed with numerous local and nonlocal side-chain interactions, and has a welldefined, dispersed NMR spectrum, which makes it possible to determine its three-dimensional structure. Most of the average interatomic distances calculated from NMR experiments are in excellent agreement with the distances from the reference replica of the T-REMD simulations (Fig. S5). Moreover, the simulations allowed us to estimate a folding free-energy difference of ~4–5 kJ/mol between HP24stab and HP24wt, which compares well with the ~3 kJ/mol free energy of denaturation obtained from the thermal melting curve. There are mechanistic explanations for the higher stability of HP24stab: 1), HP24wt shows a significant residual structure with native topology and it does not behave like random-coil; 2), the Ala mutation at residue 68 increases the helical propensity of helix 3; and 3), the hydrophobic core is stabilized by side-chain interactions between M70 and F58. Below, we discuss these three contributions in more detail.

1. Even though the CD spectrum of HP24wt shows a very characteristic random-coil-like spectrum, the NMR data unambiguously point to the presence of two very short helices connected by a rigid loop within the central part of HP24, which could be described as a residual structure in the unfolded state of HP35wt. The presence of residual structure in other truncated variants (helices 1 and 2) was also observed in previous studies (6,20,50,54,68), and thus the central part of HP35 plays a crucial role in local structuring of the unfolded state. Our NMR relaxation data show that the helices have very flexible ends but are not fully unstructured, which can be interpreted by means of a diffusing boundary model (72) of two transiently stable helices. Thus, these results indicate that the rigid central part of HP24wt serves as a nucleating scaffold, and possibly a few stabilizing interactions can easily shift the balance toward the native state. The native-state bias is also clearly observed in the ensemble of conformations generated by REMD simulations: the overlay of the representative structures of the top 10 most represented clusters shows a clear native topology (Fig. 3, C and D). The large native-state bias and the presence of residual structure also have implications for our understanding of protein energetics and protein design. In particular, long-ranged charge-charge interactions can significantly modulate the residual structure in the unfolded state, as exemplified by the recent rational design of HP35 (73). The structural bias toward the native state is in line with the funneled energy landscape and the minimum frustration principle (8,10,74).

2. Of all amino acids, alanine has the highest intrinsic helical propensity (75), and its helix-stabilizing properties help to orient the side chain of M70 toward the hydrophobic core created mainly by L61 and F58. The close proximity of M70 and F58 in HP24stab is seen in MD simulations (Fig. 3 *E*) and indicated by the presence of NOE signal between them. In contrast, the side chain of K70 in HP24wt is expelled from the hydrophobic core because the desolvation penalties are very large, which likely destabilizes the interface between helices. The high mobility and solvent accessibility of the side chain of K70 in HP24wt is nicely seen in the MD simulation (Fig. 3 *E*) and evidenced by the absence of an NOE signal between K70 and F58.

Comparison between the mechanical folding intermediate and HP24stab

Single-molecule force experiments on the hyperstable villin headpiece subdomain have required investigators to postulate an unfolding intermediate populated under load (26). This intermediate was estimated to consist of 17 residues with a folding free energy of ~10 kJ/mol. In this work, we found that the truncated HP24stab peptide, which likely resembles the core of the unfolding intermediate, has a much lower folding energy of 3 kJ/mol. A possible reason for the large difference in the folding free energies may lie in the model-dependent extrapolation used in force experiments, which provided only a rough estimate. We can also speculate that the effects of the subdomain interface and the sequential backbone-backbone interactions between a partially stretched helix 1 and the folded part of helices 2 and 3 were largely underestimated (as we previously assumed them to be negligible).

Cooperativity in protein folding and stable folded substructures

In general, the folding and unfolding of small natural proteins are highly cooperative and are often well described by a two-state model. Because of the high folding cooperativity, removing the subparts from the context of folded proteins often results in their complete unfolding. Thus, it is difficult to design small, stable protein building blocks from natural templates. To date, only a few native-like supersecondary substructures are known. The discovery of new stable substructures is of great importance (76), not only for elucidating the folding process, but also for fabricating protein nanostructures with custom-built geometries. The sparse number of stably folded substructures may also be due in part to the absence of a suitable experimental signal, which makes such substructures hard to detect using

conventional techniques. On the one hand, some experimental probes (e.g., tryptophan fluorescence) are dependent only on their local environment, and on the other hand, some global probes (CD in the peptide region) are often not sensitive enough and the presence of stable substructure is easily overlooked. Single-molecule force spectroscopy is a superb method for detecting stable substructures because the force-extension curves contain information about the folding free energies and changes in the end-to-end distance.

CONCLUSIONS

Our study of HP24stab was motivated by single-molecule force spectroscopy results that showed a deviation of the HP35stab variant from a two-state model, indicating the presence of a discrete folding intermediate (26). The structural methods and MD simulations we employed confirmed the presence of stable substructures and unraveled the molecular mechanisms that stabilize this folding intermediate, leading to the discovery (to our knowledge) of a stable supersecondary motif.

SUPPORTING MATERIAL

Supporting Materials and Methods, six figures, and six tables are available at http://www.biophysj.org/biophysj/supplemental/S0006-3495(14) 04750-X.

ACKNOWLEDGMENTS

We thank the members of our group for suggestions and comments.

This work was supported by the SFB 863/A2,A10 and ZO 291/1-1 projects of Deutsche Forschungsgemeinschaft; the Bavarian Ministry of Sciences, Research and the Arts (Bavarian Molecular Biosystems Research Network to T.M.); the German Research Foundation (Emmy Noether program MA 5703/1-1 to T.M.); and the Centre for Integrated Protein Science Munich. M.R. received support from the Nanosystems Initiative Munich. Computing time was provided by the Leibniz Supercomputing Center within Prace-0 project pr89tu and the Linux Cluster.

REFERENCES

- Chung, H. S., K. McHale, ..., W. A. Eaton. 2012. Single-molecule fluorescence experiments determine protein folding transition path times. Science. 335:981–984.
- Kubelka, J., J. Hofrichter, and W. A. Eaton. 2004. The protein folding 'speed limit'. Curr. Opin. Struct. Biol. 14:76–88.
- Lindorff-Larsen, K., S. Piana, ..., D. E. Shaw. 2011. How fast-folding proteins fold. Science. 334:517–520.
- 4. Bowler, B. E. 2012. Residual structure in unfolded proteins. *Curr. Opin. Struct. Biol.* 22:4–13.
- Cho, J. H., and D. P. Raleigh. 2009. Experimental characterization of the denatured state ensemble of proteins. *Methods Mol. Biol.* 490:339–351.
- Meng, W., B. Shan, Y. Tang, and D. P. Raleigh. 2009. Native like structure in the unfolded state of the villin headpiece helical subdomain, an ultrafast folding protein. *Protein Sci.* 18:1692–1701.

- Sosnick, T. R., and D. Barrick. 2011. The folding of single domain proteins—have we reached a consensus? *Curr. Opin. Struct. Biol.* 21:12–24.
- Bryngelson, J. D., J. N. Onuchic, ..., P. G. Wolynes. 1995. Funnels, pathways, and the energy landscape of protein folding: a synthesis. *Proteins*. 21:167–195.
- Onuchic, J. N., Z. Luthey-Schulten, and P. G. Wolynes. 1997. Theory of protein folding: the energy landscape perspective. *Annu. Rev. Phys. Chem.* 48:545–600.
- Dill, K. A., and H. S. Chan. 1997. From Levinthal to pathways to funnels. *Nat. Struct. Biol.* 4:10–19.
- 11. Lane, T. J., C. R. Schwantes, ..., V. S. Pande. 2013. Probing the origins of two-state folding. *J. Chem. Phys.* 139:145104.
- 12. Freire, E., and K. P. Murphy. 1991. Molecular basis of co-operativity in protein folding. *J. Mol. Biol.* 222:687–698.
- Hao, M. H., and H. A. Scheraga. 1998. Molecular mechanisms for cooperative folding of proteins. J. Mol. Biol. 277:973–983.
- Fleishman, S. J., and D. Baker. 2012. Role of the biomolecular energy gap in protein design, structure, and evolution. *Cell.* 149:262–273.
- Scalley-Kim, M., and D. Baker. 2004. Characterization of the folding energy landscapes of computer generated proteins suggests high folding free energy barriers and cooperativity may be consequences of natural selection. *J. Mol. Biol.* 338:573–583.
- Watters, A. L., P. Deka, ..., D. Baker. 2007. The highly cooperative folding of small naturally occurring proteins is likely the result of natural selection. Cell. 128:613–624.
- 17. Peng, Z. Y., and P. S. Kim. 1994. A protein dissection study of a molten globule. *Biochemistry*. 33:2136–2141.
- 18. Zhang, B., and Zy. Peng. 2000. A minimum folding unit in the ankyrin repeat protein p16(INK4). *J. Mol. Biol.* 299:1121–1132.
- Brown, J. E., and W. A. Klee. 1971. Helix-coil transition of the isolated amino terminus of ribonuclease. *Biochemistry*. 10:470–476.
- Bierzynski, A., P. S. Kim, and R. L. Baldwin. 1982. A salt bridge stabilizes the helix formed by isolated C-peptide of RNase A. *Proc. Natl. Acad. Sci. USA*. 79:2470–2474.
- D'Aquino, J. A., J. Gómez, ..., E. Freire. 1996. The magnitude of the backbone conformational entropy change in protein folding. *Proteins*. 25:143–156.
- Khurana, S., and S. P. George. 2008. Regulation of cell structure and function by actin-binding proteins: villin's perspective. *FEBS Lett*. 582:2128–2139.
- Meng, J., D. Vardar, ..., C. J. McKnight. 2005. High-resolution crystal structures of villin headpiece and mutants with reduced F-actin binding activity. *Biochemistry*. 44:11963–11973.
- 24. McKnight, C. J., D. S. Doering, ..., P. S. Kim. 1996. A thermostable 35-residue subdomain within villin headpiece. *J. Mol. Biol.* 260: 126–134.
- Bi, Y., J. H. Cho, ..., D. P. Raleigh. 2007. Rational design, structural and thermodynamic characterization of a hyperstable variant of the villin headpiece helical subdomain. *Biochemistry*. 46:7497–7505.
- Žoldák, G., J. Stigler, ..., M. Rief. 2013. Ultrafast folding kinetics and cooperativity of villin headpiece in single-molecule force spectroscopy. *Proc. Natl. Acad. Sci. USA*. 110:18156–18161.
- Mayr, L. M., O. Landt, ..., F. X. Schmid. 1993. Stability and folding kinetics of ribonuclease T1 are strongly altered by the replacement of cis-proline 39 with alanine. J. Mol. Biol. 231:897–912.
- Wishart, D. S., C. G. Bigam, ..., B. D. Sykes. 1995. 1H, 13C and 15N chemical shift referencing in biomolecular NMR. *J. Biomol. NMR*. 6:135–140.
- Yuwen, T., and N. R. Skrynnikov. 2014. Proton-decoupled CPMG: a better experiment for measuring (15)N R2 relaxation in disordered proteins. J. Magn. Reson. 241:155–169.
- 30. Vranken, W. F., W. Boucher, ..., E. D. Laue. 2005. The CCPN data model for NMR spectroscopy: development of a software pipeline. *Proteins*. 59:687–696.

686 Hocking et al.

 Güntert, P., C. Mumenthaler, and K. Wüthrich. 1997. Torsion angle dynamics for NMR structure calculation with the new program DYANA. J. Mol. Biol. 273:283–298.

- Shen, Y., and A. Bax. 2013. Protein backbone and sidechain torsion angles predicted from NMR chemical shifts using artificial neural networks. J. Biomol. NMR. 56:227–241.
- Nederveen, A. J., J. F. Doreleijers, ..., A. M. Bonvin. 2005.
 RECOORD: a recalculated coordinate database of 500+ proteins from the PDB using restraints from the BioMagResBank. *Proteins*. 59:662–672.
- Doreleijers, J. F., A. W. Sousa da Silva, ..., G. W. Vuister. 2012.
 CING: an integrated residue-based structure validation program suite.
 J. Biomol. NMR. 54:267–283.
- Svergun, D. I. 1992. Determination of the regularization parameter in indirect-transform methods using perceptual criteria. *J. Appl. Cryst.* 25:495–503.
- Bergmann, A., G. Fritz, and O. Glatter. 2000. Solving the generalized indirect Fourier transformation (GIFT) by Boltzmann simplex simulated annealing (BSSA). J. Appl. Cryst. 33:1212–1216.
- Franke, D., and D. I. Svergun. 2009. DAMMIF, a program for rapid abinitio shape determination in small-angle scattering. *J. Appl. Cryst.* 42:342–346.
- 38. Volkov, V. V., and D. I. Svergun. 2003. Uniqueness of ab initio shape determination in small-angle scattering. *J. Appl. Cryst.* 36:860–864.
- van der Spoel, D., E. Lindahl, ..., H. J. C. Berendsen. 2010. GROMACS User Manual, version 4.5. http://www.gromacs.org.
- Lindorff-Larsen, K., S. Piana, ..., D. E. Shaw. 2010. Improved sidechain torsion potentials for the Amber ff99SB protein force field. *Proteins*. 78:1950–1958.
- Schroedinger, L. 2010. The PyMOL Molecular Graphics System, version 1.3r1. Schrödinger LLC.
- Jorgensen, W. L., J. Chandrasekhar, ..., M. L. Klein. 1983. Comparison of simple potential functions for simulating liquid water. *J. Chem. Phys.* 79:926–935.
- Patriksson, A., and D. van der Spoel. 2008. A temperature predictor for parallel tempering simulations. *Phys. Chem. Chem. Phys.* 10:2073– 2077
- 44. Daura, X., K. Gademann, ..., A. E. Mark. 1999. Peptide folding: when simulation meets experiment. *Angew. Chem. Int. Ed.* 38:236–240.
- Souaille, M., and B. Roux. 2001. Extension to the weighted histogram analysis method: combining umbrella sampling with free energy calculations. Comput. Phys. Commun. 135:40–57.
- Whitmore, L., and B. A. Wallace. 2004. DICHROWEB, an online server for protein secondary structure analyses from circular dichroism spectroscopic data. *Nucleic Acids Res.* 32:W668–W673.
- Whitmore, L., and B. A. Wallace. 2008. Protein secondary structure analyses from circular dichroism spectroscopy: methods and reference databases. *Biopolymers*. 89:392–400.
- 48. Duan, Y., and P. A. Kollman. 1998. Pathways to a protein folding intermediate observed in a 1-microsecond simulation in aqueous solution. *Science*. 282:740–744.
- Kubelka, J., W. A. Eaton, and J. Hofrichter. 2003. Experimental tests of villin subdomain folding simulations. J. Mol. Biol. 329:625–630.
- Tang, Y., D. J. Rigotti, ..., D. P. Raleigh. 2004. Peptide models provide evidence for significant structure in the denatured state of a rapidly folding protein: the villin headpiece subdomain. *Biochemistry*. 43:3264–3272.
- Chiu, T. K., J. Kubelka, ..., D. R. Davies. 2005. High-resolution x-ray crystal structures of the villin headpiece subdomain, an ultrafast folding protein. *Proc. Natl. Acad. Sci. USA*. 102:7517–7522.
- 52. Kubelka, J., T. K. Chiu, ..., J. Hofrichter. 2006. Sub-microsecond protein folding. J. Mol. Biol. 359:546–553.
- 53. Tang, Y., M. J. Grey, ..., D. P. Raleigh. 2006. Multistate folding of the villin headpiece domain. *J. Mol. Biol.* 355:1066–1077.

 Tang, Y., M. J. Goger, and D. P. Raleigh. 2006. NMR characterization of a peptide model provides evidence for significant structure in the unfolded state of the villin headpiece helical subdomain. *Biochemistry*. 45:6940–6946.

- Cellmer, T., E. R. Henry, ..., W. A. Eaton. 2007. Relaxation rate for an ultrafast folding protein is independent of chemical denaturant concentration. J. Am. Chem. Soc. 129:14564–14565.
- Lei, H., and Y. Duan. 2007. Two-stage folding of HP-35 from ab initio simulations. J. Mol. Biol. 370:196–206.
- Freddolino, P. L., and K. Schulten. 2009. Common structural transitions in explicit-solvent simulations of villin headpiece folding. *Biophys. J.* 97:2338–2347.
- Reiner, A., P. Henklein, and T. Kiefhaber. 2010. An unlocking/relocking barrier in conformational fluctuations of villin headpiece subdomain. *Proc. Natl. Acad. Sci. USA*. 107:4955–4960.
- Urbanek, D. C., D. Y. Vorobyev, ..., R. M. Hochstrasser. 2010. The two dimensional vibrational echo of a nitrile probe of the villin HP35 protein. J. Phys. Chem. Lett. 1:3311–3315.
- Lei, H., Y. Su, ..., Y. Duan. 2010. Folding network of villin headpiece subdomain. *Biophys. J.* 99:3374–3384.
- Zhu, L., K. Ghosh, ..., L. J. Lapidus. 2011. Evidence of multiple folding pathways for the villin headpiece subdomain. *J. Phys. Chem.* B. 115:12632–12637.
- Beauchamp, K. A., D. L. Ensign, ..., V. S. Pande. 2011. Quantitative comparison of villin headpiece subdomain simulations and triplettriplet energy transfer experiments. *Proc. Natl. Acad. Sci. USA*. 108:12734–12739.
- 63. Lei, H., C. Chen, ..., Y. Duan. 2011. The protein folding network indicates that the ultrafast folding mutant of villin headpiece subdomain has a deeper folding funnel. *J. Chem. Phys.* 134:205104.
- 64. Jani, V., U. B. Sonavane, and R. Joshi. 2011. Microsecond scale replica exchange molecular dynamic simulation of villin headpiece: an insight into the folding landscape. *J. Biomol. Struct. Dyn.* 28:845–860.
- Chung, J. K., M. C. Thielges, and M. D. Fayer. 2011. Dynamics of the folded and unfolded villin headpiece (HP35) measured with ultrafast 2D IR vibrational echo spectroscopy. *Proc. Natl. Acad. Sci. USA*. 108:3578–3583.
- Piana, S., K. Lindorff-Larsen, and D. E. Shaw. 2012. Protein folding kinetics and thermodynamics from atomistic simulation. *Proc. Natl.* Acad. Sci. USA. 109:17845–17850.
- Serrano, A. L., O. Bilsel, and F. Gai. 2012. Native state conformational heterogeneity of HP35 revealed by time-resolved FRET. *J. Phys. Chem. B.* 116:10631–10638.
- Wickstrom, L., A. Okur, ..., C. L. Simmerling. 2006. The unfolded state of the villin headpiece helical subdomain: computational studies of the role of locally stabilized structure. *J. Mol. Biol.* 360:1094–1107.
- Herges, T., and W. Wenzel. 2004. An all-atom force field for tertiary structure prediction of helical proteins. *Biophys. J.* 87:3100–3109.
- Neidigh, J. W., R. M. Fesinmeyer, and N. H. Andersen. 2002. Designing a 20-residue protein. *Nat. Struct. Biol.* 9:425–430.
- Kortemme, T., M. Ramírez-Alvarado, and L. Serrano. 1998. Design of a 20-amino acid, three-stranded β-sheet protein. Science. 281:253–256.
- Neumaier, S., A. Reiner, ..., T. Kiefhaber. 2013. Testing the diffusing boundary model for the helix-coil transition in peptides. *Proc. Natl. Acad. Sci. USA*. 110:12905–12910.
- Xiao, S., V. Patsalo, ..., D. P. Raleigh. 2013. Rational modification of protein stability by targeting surface sites leads to complicated results. *Proc. Natl. Acad. Sci. USA*. 110:11337–11342.
- 74. Go, N. 1983. Theoretical studies of protein folding. *Annu. Rev. Biophys. Bioeng.* 12:183–210.
- Spek, E. J., C. A. Olson, ..., N. R. Kallenbach. 1999. Alanine is an intrinsic α-helix stabilizing amino acid. *J. Am. Chem. Soc.* 121: 5571–5572
- Imperiali, B., and J. J. Ottesen. 1999. Uniquely folded mini-protein motifs. J. Pept. Res. 54:177–184.